



# Piezoelectricity enhances MoSe<sub>2</sub> nanoflowers adsorption of the antibacterial dye malachite green under sonication

Jinzhu Wu<sup>1</sup> · Beibei Li<sup>1</sup> · Yanbin Shao<sup>2</sup> · Xiaohong Wu<sup>1</sup> · Wenjie Zhao<sup>3</sup>

Received: 6 March 2020 / Accepted: 30 June 2020 / Published online: 8 July 2020  
© Springer Nature Switzerland AG 2020

## Abstract

Nanoscale piezoelectrics have recently found applications in radios, switches, tweezers, sensors, actuators, field effect transistors and piezoelectric-gated diodes. Piezoelectrics may also be used to adsorb and efficiently degrade pollutants, yet knowledge is actually scarce. Two-dimensional transition metal dichalcogenides were recently found to be piezoelectric. Here, MoSe<sub>2</sub> nanoflowers were synthesized by the hydrothermal method then used to adsorb the malachite green dye, an antifungal and antibacterial agent for aquaculture. Results show very high dye adsorption, of 85% within 5 s under sonication, with a theoretical maximum adsorption capacity of 208.3 mg g<sup>-1</sup>. This is explained by spontaneous physisorption via  $\pi$ - $\pi$  stacking interactions between aromatic malachite green and electron-rich MoSe<sub>2</sub> nanoflowers. For the first time, this work clarifies that the piezoelectric effect of the few-layered MoSe<sub>2</sub> nanoflowers triggered by the ultrasonic vibration is a driven force for outstanding adsorption.

**Keywords** Piezoelectric effect · MoSe<sub>2</sub> · 2D materials · Adsorption · Nanomaterial · Pesticide · Dye removal

## Introduction

Piezoelectric materials have been used in many conventional fields, but the novel ones are still in urgent needs especially for next-generation nanoscale piezoelectric devices (Zheng

et al. 2017; Zhang 2019; Duerloo et al. 2012). Currently, low-dimensional materials such as nanoparticles, nanotubes and nanosheets have been utilized in the nanoscale piezoelectrics including radios (Jensen et al. 2007), switches (Lee et al. 2004), tweezers (Zhang 2019), sensor (Stampfer et al. 2006), actuators (Eddingsaas and Suslick 2006), field effect transistors (Zheng et al. 2017) and piezoelectric-gated diodes (Duerloo et al. 2012), where controllable charges and electric fields induced by mechanical stimuli play a key role in their application performance.

Graphene and certain two-dimensional (2D) trigonal prismatic coordinated transition metal dichalcogenides are intrinsically piezoelectric (Duerloo and Reed 2015; Wu et al. 2014; Ong and Reed 2012). Molybdenum diselenide (MoSe<sub>2</sub>) is a typical transition metal dichalcogenide with a non-centrosymmetric structure, which is required for the piezoelectric materials. As expected, the single- and odd few-layered MoSe<sub>2</sub> present superior piezoelectricity over the bulk counterpart and some popular wurtzite crystals (Li and Li 2015; Milošević et al. 2007). That is to say, once they are subjected to a mechanical force, they may show piezoelectric activity due to electromechanical coupling effect induced.

Wu et al. (2017) demonstrated the superhigh piezocatalytic activity of the single- and few-layered MoSe<sub>2</sub> nanoflowers for decomposing rhodamine B. They found that these MoSe<sub>2</sub>

**Electronic supplementary material** The online version of this article (<https://doi.org/10.1007/s10311-020-01048-z>) contains supplementary material, which is available to authorized users.

✉ Jinzhu Wu  
wujinzhu@hit.edu.cn

✉ Xiaohong Wu

✉ Wenjie Zhao

<sup>1</sup> Department of Materials Chemistry, School of Chemistry and Chemical Engineering, Harbin Institute of Technology, 92 West Dazhi Street, Nan Gang District, Harbin 150006, People's Republic of China

<sup>2</sup> The Academy of Fundamental and Interdisciplinary Sciences, Harbin Institute of Technology, 92 West Dazhi Street, Nan Gang District, Harbin 150006, People's Republic of China

<sup>3</sup> The Higher Educational Key Laboratory for Measuring and Control Technology and Instrumentations of Heilongjiang Province, Harbin University of Science and Technology, 52 Xuefu Road, Nan Gang District, Harbin 150080, People's Republic of China

nanoflowers (10 mg) can successfully decompose rhodamine B (about 45 mg) in 30 s under ultrasonic vibration in dark. They used piezoresponse force microscope and tunneling atomic force microscope to successfully record piezoelectric potential created by a MoSe<sub>2</sub> nanosheet. Interestingly, Hu et al. reported an impressive adsorption ability of the MoSe<sub>2</sub> nanosheets to rhodamine B (15 mg L<sup>-1</sup>) with an equilibrium adsorption capacity of 133 mg g<sup>-1</sup> in 5 min, which is comparable to that of activated carbon in 20 min (Jiang et al. 2017). It should be mentioned that for this adsorption experiment, no external mechanical force was employed besides stirring at a rate of 300 rpm. The above two representative studies raise few questions about the few-layered MoSe<sub>2</sub>: (1) What is the adsorption performance under ultrasonic vibration? (2) Is the induced piezoelectric effect beneficial for adsorption, as for catalysis?

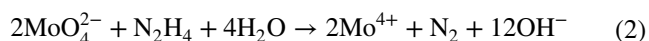
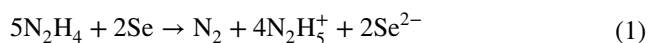
To address these issues, here we synthesized the few-layered MoSe<sub>2</sub> nanoflowers by using a simple hydrothermal method and then explored their adsorption performance toward malachite green under ultrasonic vibration. Malachite green is a commonly used green organic dye as well as an antiparasitic, antifungal and antibacterial agent in aquaculture, although it is toxic and carcinogenic (Wu et al. 2011a, b).

## Experimental

### Hydrothermal synthesis of the few-layered MoSe<sub>2</sub> nanoflowers

Hydrazine hydrate solution (N<sub>2</sub>H<sub>4</sub>·H<sub>2</sub>O, 85.0%), sodium molybdate (Na<sub>2</sub>MoO<sub>4</sub>·2H<sub>2</sub>O, 99.99%) and selenium powder (Se, 99.99%) were purchased from Sigma-Aldrich and used as received. Deionized water was used throughout experiments.

0.3693 g of Na<sub>2</sub>MoO<sub>4</sub>·2H<sub>2</sub>O was dissolved in 25 mL of distilled water. 0.3590 g of Se powder was added into 15 mL of hydrazine hydrate solution with strong agitation, and then the resulting solution was dropped into the above solution to make a clear orange-red solution with a molar ratio of Mo/Se of about 1:2. Thereafter, the solution was transferred into a Teflon-lined autoclave (50 mL) and heated at 180 °C for 24 h. After being cooled to room temperature, the precipitate was centrifuged and washed with absolute ethanol and deionized water several times and then vacuum-dried. Figure S1 shows the schematic illustration of the synthetic process, which involves the following reactions (Wu et al. 2020):



## Characterization

X-ray diffractometer (XRD, Rigaku D/Max-2400, Cu K<sub>α</sub> radiation) was used to examine the crystalline information of the samples. Raman spectra of the samples were recorded on Renishaw inVia with 532 nm laser. The chemical composition and bonding state of the samples were analyzed by X-ray photoelectron spectroscopy (XPS, PHI 5000 Versa Probe, Mg K<sub>α</sub> radiation) and Fourier transform infrared spectrometry (FTIR, Hitachi UH4150). Morphology of the samples was observed by field-emission scanning electron microscopy (SEM, Hitachi SU8000) and transmission electron microscopy (TEM, JEOL JEM-2010).

## Measurement of piezoelectric potential

Piezoelectric current was measured by using an electrochemical workstation (CHI Instrument 660E) with a standard three-electrode setup, where the MoSe<sub>2</sub> nanoflowers as a working electrode in deionized water, platinum (Pt) foil as a counter electrode and Ag/AgCl as a reference electrode, respectively.

## Ultrasonic assisted adsorption and kinetic study

Adsorption performance of the MoSe<sub>2</sub> nanoflowers (0.2 g L<sup>-1</sup>) toward malachite green (30, 35 and 40 mg L<sup>-1</sup>) under ultrasonic vibration was estimated by measuring UV–Vis absorption spectra with UV–Vis spectrophotometer (METASH-8000S).

Adsorption kinetic study was conducted based on Lagergren's pseudo-first-order and pseudo-second-order models given by the following equations (Uslu et al. 2017; Xu et al. 2012; Wu et al. 2011a, b):

$$\text{pseudo - first - order: } \ln(q_e - q_t) = \ln q_e - k_1 t$$

$$\text{pseudo - second - order: } t/q_t = 1/k_2 q_e + 1/q_e$$

where  $q_e$  and  $q_t$  (mg g<sup>-1</sup>) are adsorption capacities at equilibrium and at time  $t$ , respectively, and  $k_1$  (s<sup>-1</sup>) and  $k_2$  (g mg<sup>-1</sup> s<sup>-1</sup>) are the corresponding rate constants.

Four adsorption models (i.e., Langmuir, Temkin, Freundlich and Dubinin–Radushkevich) were used to describe equilibrium adsorption data. Langmuir adsorption isotherm model is the description of monolayer adsorption on an energetically uniform surface with finite adsorption sites. The linear form of Langmuir model is given by Eq. (4) (ConsoLin-Filho et al. 2010; Kong et al. 2020):

$$\frac{C_e}{q_e} = \frac{1}{k_1 q_m} + \frac{1}{q_m} C_e \quad (4)$$

where  $C_e$  is the concentration of malachite green solution at equilibrium ( $\text{mg L}^{-1}$ ),  $q_e$  is the amount of malachite green per mass of adsorbent at equilibrium ( $\text{mg g}^{-1}$ ),  $k_1$  is Langmuir constant ( $\text{L mg}^{-1}$ ) that represents the affinity between adsorbate and adsorbent and  $q_m$  is the maximum adsorption capacity for monolayer coverage ( $\text{mg g}^{-1}$ ).

Temkin isotherm model assumes uniform distribution of heterogeneous binding sites and an adsorption enthalpy that varies due to the heterogeneity of sites. This model is presented in Eq. (5) (Anirudhan and Radhakrishnan 2011; Uslu et al. 2017):

$$q_e = a \ln k_t + a \ln C_e \quad (5)$$

where  $k_t$  ( $\text{L mg}^{-1}$ ) and  $a$  are Temkin constant related to the initial adsorption heat and the surface heterogeneity of the adsorbent, respectively.

Freundlich isotherm model is an empirical equation based on the assumption of heterogeneous adsorption, and it is suitable to describe both monolayer and multilayer adsorption. Freundlich isotherm is expressed in Eq. (6) (Wu et al. 2011a, b; Uslu et al. 2017):

$$\ln q_e = \ln k_f + \frac{1}{n} \ln C_e \quad (6)$$

where  $k_f$  ( $\text{mg g}^{-1} (\text{L mg}^{-1})^{1/n}$ ) and  $n$  are the Freundlich constants related to the adsorption capacity and adsorption intensity of the adsorbent, respectively.

For liquid–solid phase adsorption, the amount adsorbed corresponding to any adsorbate concentration is assumed to be a Gaussian function of the Polanyi potential,  $\varepsilon$ . This Dubinin–Radushkevich isotherm model is presented in Eqs. (7) and (8) (Uslu et al. 2017):

$$\ln q_e = \ln q_m - k_{D-R} \varepsilon^2 \quad (7)$$

$$\varepsilon = RT \ln \left( 1 + \frac{1}{C_e} \right) \quad (8)$$

where  $q_e$  is the amount of malachite green per mass of adsorbent at equilibrium ( $\text{mol g}^{-1}$ ),  $q_m$  is the maximum adsorption capacity at monolayer coverage ( $\text{mol g}^{-1}$ ),  $C_e$  is the concentration of malachite green solution at equilibrium ( $\text{mol L}^{-1}$ ),  $k_{D-R}$  is a constant related to sorption energy ( $\text{mol}^2 \text{kJ}^{-2}$ ),  $\varepsilon$  is the Polanyi potential ( $\text{kJ}^2 \text{mol}^{-2}$ ),  $T$  is absolute temperature ( $\text{K}$ ) and  $R$  is the universal gas constant ( $8.314 \text{ J mol}^{-1} \text{ K}^{-1}$ ).

### Adsorption thermodynamic study

For adsorption thermodynamic study, experiments were conducted at 303.15, 313.15 and 323.15 K, respectively. The

thermodynamic parameters can be calculated by the van't Hoff Eq. (9) (Prathap and Namasivayam 2010):

$$\ln \left( \frac{q_e}{C_e} \right) = -\frac{\Delta H}{RT} + \frac{\Delta S}{R} \quad (9)$$

Plotting  $\ln(q_e/C_e)$  against  $1/T$  gives a straight line with slope and intercept equal to  $-\Delta H/R$  and  $\Delta S/R$ , respectively.

Gibbs free energy change ( $\Delta G$ ) can be calculated from the following relation Eq. (10) (Prathap and Namasivayam 2010):

$$\Delta G = \Delta H - T\Delta S \quad (10)$$

where  $T$  is absolute temperature ( $\text{K}$ ) and  $R$  is the universal gas constant.  $\Delta H$  ( $\text{kJ mol}^{-1}$ ) and  $\Delta S$  ( $\text{J mol}^{-1} \text{ K}^{-1}$ ) are enthalpy change and entropy change, respectively.

## Results and discussion

Scanning electron microscopy (SEM) and transmission electron microscopy (TEM) images of the synthesized  $\text{MoSe}_2$ , shown in Fig. 1a, b display a nanoflower-like morphology composed of outstretched  $\text{MoSe}_2$  nanosheets. High-resolution TEM image shown in Fig. 1c clearly reveals that the  $\text{MoSe}_2$  nanosheets possess few-layered structure with inter-layer spacing ( $d$ ) of around 0.85 nm, larger than 0.64 nm for the bulk counterpart (Yin et al. 2017). It also shows a characteristic honeycomb-like atomic spatial arrangement of Mo and Se atoms, which corresponds to 2H phase (Fig. 1c inset) (Nath and Rao 2001).

The X-ray diffraction (XRD) pattern of the few-layered  $\text{MoSe}_2$  nanoflowers, shown in Fig. 1d, is comparable to standard 2H- $\text{MoSe}_2$  (PDF no. 29-0914) except a left-shifted diffraction peak at  $2\theta = 10^\circ$  corresponding to (002) plane and a right-shifted one at  $2\theta = 33^\circ$  corresponding to (100) plane. The calculated  $d$  value of (002) plane by Bragg equation was about 0.85 nm, well consistent with the above HRTEM observation. Although the distorted (002) and (100) planes exist due to the limited number of layers, the current  $\text{MoSe}_2$  nanoflowers are well crystalline. The aforementioned changed crystalline structure may endow the  $\text{MoSe}_2$  nanoflowers with an out-of-plane uniaxial tensile strain along  $c$  direction and in-plane biaxial compressive strain in horizontal plane (Fig. 1d insets), respectively (Xu et al. 2012). Therefore, the few-layered  $\text{MoSe}_2$  nanoflowers may be vulnerable to an external force and thus make response such as piezoresponse. Furthermore, the relevant Raman and XPS spectra shown in Fig. S2 confirm again the synthesis of the few-layered 2H- $\text{MoSe}_2$  with a certain degree of lattice distortion.

In order to explore the possible piezoelectric effect induced by the ultrasonic vibration, the output current of

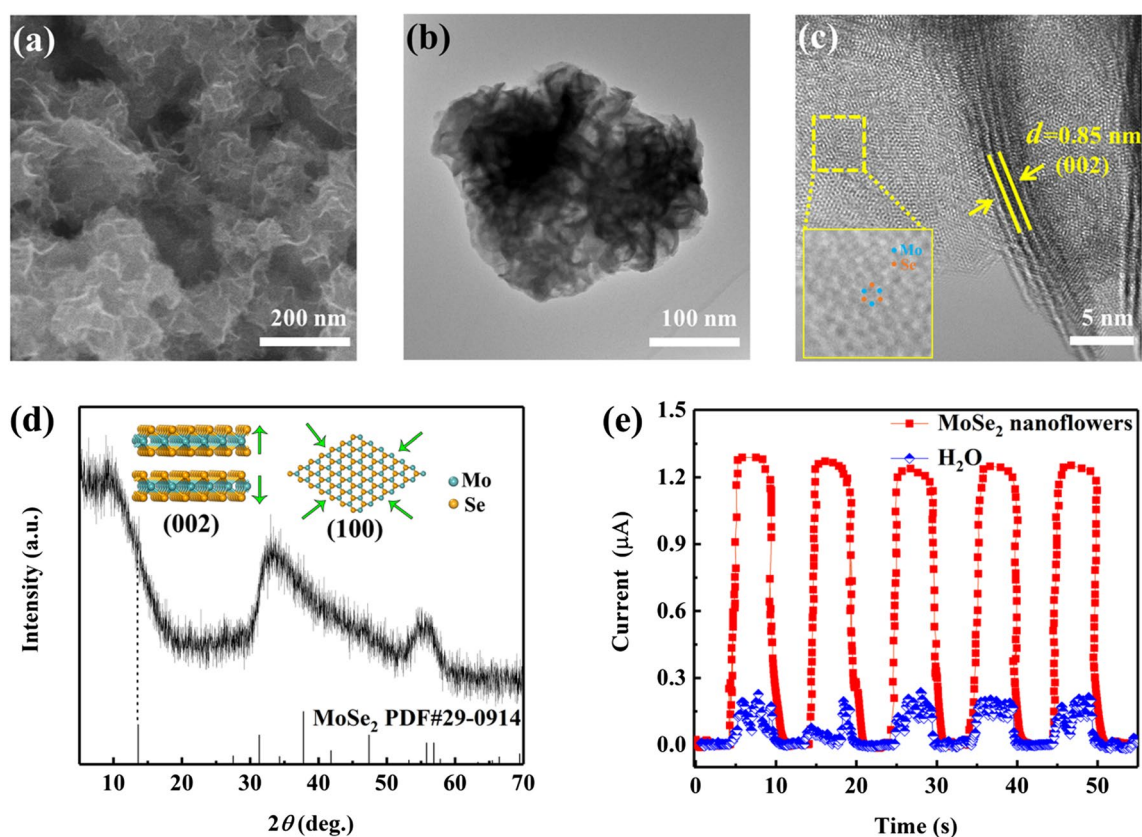


**Fig. 1** **a** Scanning electron microscopy (SEM) image, **b** transmission electron microscopy (TEM) image, **c** high-resolution transmission electron microscopy (HRTEM) image, and **d** X-ray diffraction (XRD) pattern of the MoSe<sub>2</sub> nanoflowers. Inset in **c** is an enlarged image of the arrangement of Mo and Se atoms for 2H phase (honeycomb). **e**

Current of the MoSe<sub>2</sub> nanoflowers under ultrasonic vibration measured by an electrochemical workstation. Note that the as-synthesized MoSe<sub>2</sub> possesses 2H phase and few-layered structure with enlarged interlayer spacing, which presents a piezoelectric effect induced by the ultrasonic vibration

the MoSe<sub>2</sub> nanoflowers dispersed in deionized water was measured by an electrochemical workstation shown in Fig. 1e. Clearly, once the sonicator was turned on, up to 1.3 μA of the output current was recorded. Otherwise, the output current did not occur. In order to identify the current is truly originated from the piezoelectric property of the few-layered MoSe<sub>2</sub> nanoflowers. The deionized water under ultrasonic vibration was tested for comparison, and the current was hardly acquired. These findings suggest the obvious piezoresponse of the MoSe<sub>2</sub> nanoflowers in response to the ultrasonic vibration as a mechanical force. Generally, piezoresponse force microscope (PFM) and tunneling atomic force microscope (TUNA) are used to characterize the piezoelectric response and resulting current distribution of 2D materials. Xu et al. reported different polarization orientation and piezoelectric responsive potential of the MoSe<sub>2</sub> nanoflowers by using PFM and TUNA (Xu et al. 2012). These techniques require that the samples should be in a dry state. Alternatively, in this work, for the first time, mass MoSe<sub>2</sub> nanoflowers in a medium are directly analyzed by using the electrochemical workstation for their piezoelectric

effect. This analytical method is of significance, because it is straightforward, cost-efficient and convenient.

The adsorption performance of the MoSe<sub>2</sub> nanoflowers toward malachite green was evaluated. Adsorption process involves mass transfer of the malachite green from aqueous phase to the surfaces of the MoSe<sub>2</sub> nanoflowers. Figure 2a and b shows UV–Vis absorption spectra of the malachite green aqueous solution (30 mg L<sup>-1</sup>) with the MoSe<sub>2</sub> nanoflowers under stir or ultrasonic vibration for different times, showing a characteristic absorption band at 617 nm. It is obvious that the adsorption of the malachite green on the MoSe<sub>2</sub> nanoflowers under ultrasonic vibration is significantly efficient over that under stir. As can be seen, nearly 90% of malachite green have been removed by the MoSe<sub>2</sub> nanoflowers in 30 s of the ultrasonic treatment. Furthermore, both adsorption processes follow a time-dependent manner. In contrast, the commercial MoSe<sub>2</sub> flakes do not have obvious adsorption effect on the malachite green after stirring and ultrasonic treatments (Fig. S3a and b).

Figure 2c gives the adsorption time profile of the malachite green (30 mg L<sup>-1</sup>) onto the MoSe<sub>2</sub> nanoflowers. As

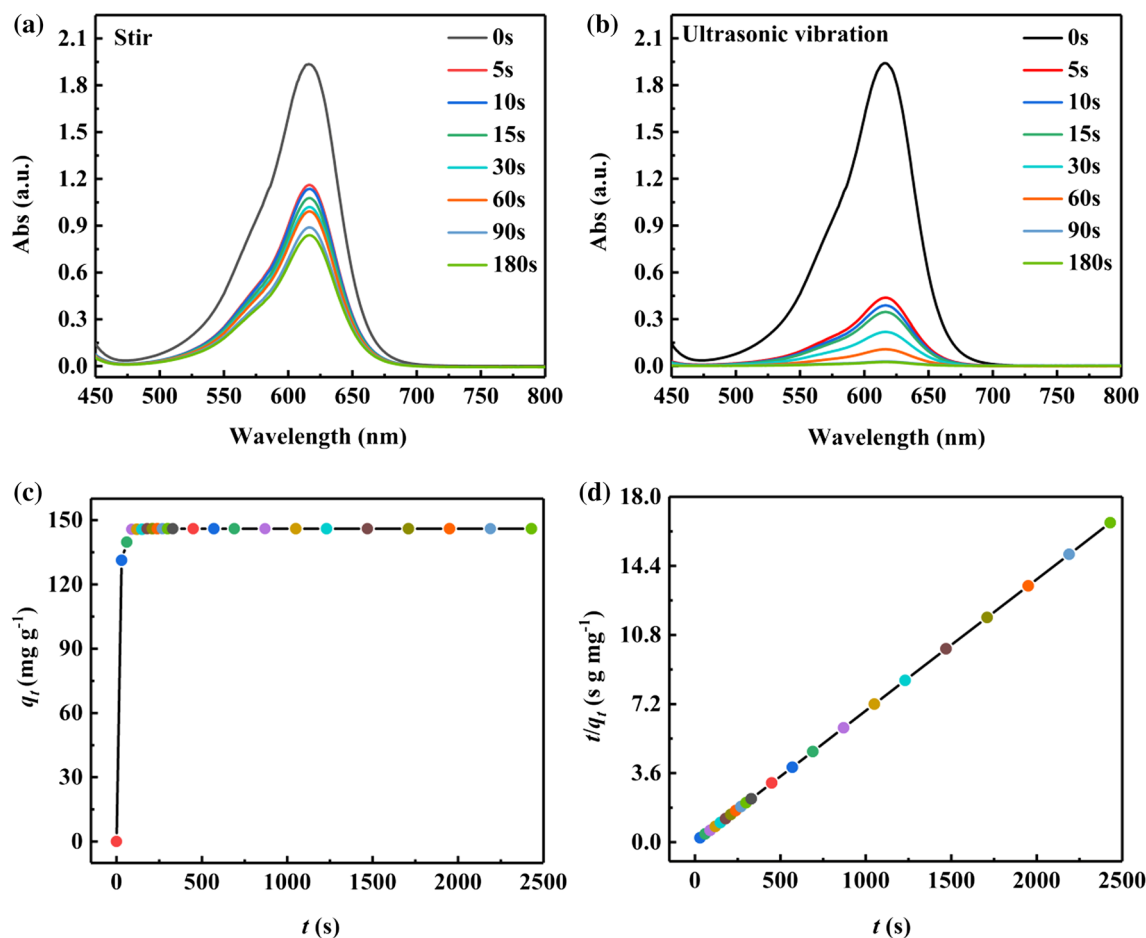


**Fig. 2** A typical adsorption process of malachite green ( $30 \text{ mg L}^{-1}$ ) on  $\text{MoSe}_2$  nanoflowers measured by ultraviolet–visible (UV–Vis) spectroscope under **a** stir and **b** ultrasonic vibration. Note the ultrafast and highly efficient adsorption of the malachite green on the  $\text{MoSe}_2$  nanoflowers under ultrasonic vibration with the adsorption efficiency

of 85% in 5 s and nearly 100% in 180 s. **c** The adsorption time profile of the malachite green on the  $\text{MoSe}_2$  nanoflowers. Note that initially the adsorption increases quickly with time and soon reaches saturation, well fitted with **d** pseudo-second-order kinetic curve following a linear equation of  $t/q_t = 0.00685t + 0.00408$  ( $R^2 = 0.99$ )

can be seen, the adsorption immediately takes place once the ultrasonic vibration is employed and then reaches its equilibrium in a short time of 3 min. The adsorption capacities are  $131 \text{ mg g}^{-1}$  at 30 s and  $146 \text{ mg g}^{-1}$  at equilibrium. Kinetic study can provide important information about corresponding adsorption mechanisms. Figure 2d shows the adsorption kinetic curve, which well obeys a pseudo-second-order rate equation ( $R^2 = 0.99$ ) instead of a pseudo-first-order one (Fig. S4). The adsorption rate constant ( $k_2$ ) is  $0.69 \text{ g mg}^{-1} \text{ min}^{-1}$ , which is a very high value to our knowledge. Further kinetic studies about the adsorption of the malachite green with different initial concentrations ( $35$  and  $40 \text{ mg L}^{-1}$ ) onto the  $\text{MoSe}_2$  nanoflowers are shown in Fig. S5a–f, confirming the above findings. The pseudo-second-order kinetics suggests that the adsorption rate is mainly controlled by the adsorption mechanism (Xu et al. 2012). This is the first report about boosting the adsorption performance of the few-layered  $\text{MoSe}_2$  nanoflowers by the ultrasonic vibration.

It is well known that surface area is an exclusive factor to determine the adsorption ability of the adsorbents. By analyzing nitrogen adsorption–desorption isotherms of the as-synthesized  $\text{MoSe}_2$  nanoflowers shown in Fig. S6a, they feature the large specific surface area ( $39 \text{ m}^2 \text{ g}^{-1}$ ) and hierarchical mesoporosity from 2 to 30 nm (Fig. S6b), which contribute to the efficient adsorption.

To clarify the adsorption behaviors of the  $\text{MoSe}_2$  nanoflowers, appropriate adsorption isotherms were simulated by using four models, as shown in Table 1, where  $k$  is an adsorption constant and  $q_m$  is the maximum adsorption capacity. Langmuir model is an ideal homogeneous monolayer adsorption on the surfaces with identical sites. Temkin model is a modified monolayer adsorption based on Langmuir model. Freundlich model describes heterogeneous multilayer adsorption, in which  $1/n$  is calculated from the intercept and slope of the linear plot of  $\ln q_e$  versus  $\ln C_e$ . Dubinin–Radushkevich model concerns the adsorption onto

**Table 1** Regression parameters of adsorption isotherms fitted by four typical models

Parameter	Model			
	Langmuir	Temkin	Freundlich	Dubinin–Radushkevich
$R^2$	0.99	0.85	0.83	0.83
$k$	1.13 (L mg <sup>-1</sup> )	98.72 (L mg <sup>-1</sup> )	127.70 (mg g <sup>-1</sup> (L mg <sup>-1</sup> ) <sup>1/n</sup> ) <sup>a</sup>	1.18 × 10 <sup>-3</sup> (mol <sup>2</sup> kJ <sup>-2</sup> )
$q_m$ (mg g <sup>-1</sup> )	208.30	27.64	Not applicable	1.20 × 10 <sup>-3</sup>

Note that the adsorption of the malachite green on the MoSe<sub>2</sub> nanoflowers abides by Langmuir model ( $R^2=0.99$ )

<sup>a</sup> $n=5.69$

the special porous materials. By comparing the correlation coefficient ( $R^2$ ) of these models, it may be concluded that the adsorption of the malachite green onto the MoSe<sub>2</sub> nanoflowers abides by Langmuir model with a theoretical maximum adsorption capacity of 208.3 mg g<sup>-1</sup>.

The thermodynamic analysis of the adsorption process was performed as shown in Table S1 to better understand its possibility. The negative standard free energy changes ( $\Delta G^\theta$ ) suggest that the adsorption at different temperatures was a spontaneous process. Furthermore, the adsorption with  $\Delta G^\theta$  values in the range of  $-20$  to  $0$  kJ mol<sup>-1</sup> corresponds to spontaneous physisorption processes, while those with  $-400$  to  $-80$  kJ mol<sup>-1</sup> of  $\Delta G^\theta$  values refer to chemisorption processes (Timóteo et al. 2020). Therefore, the adsorption of the malachite green on the MoSe<sub>2</sub> nanoflowers may be spontaneous physisorption process. Assuming constant standard enthalpy changes ( $\Delta H^\theta$ ) and standard entropy changes ( $\Delta S^\theta$ ) for the adsorption processes within the experimental temperature range, the respective negative values reveal that the adsorption process is exothermic in which the randomness of the solid–liquid interfaces becomes decreased.

Some adsorption mechanisms have been proposed such as electrostatic interaction, coordination/chelation bonding, hydrogen bonding and  $\pi$ – $\pi$  interaction (Wu et al. 2011a, b; Hazafy et al. 2011). When a piezoelectric voltage is generated, the induced negative charges are preserved on the surfaces of the *n*-type semiconductive MoSe<sub>2</sub> nanosheets. Considering the complicated aromatic ring in the MG molecule, we suppose that the electrostatic interaction and/or  $\pi$ – $\pi$  interaction between the malachite green as an electron acceptor and the MoSe<sub>2</sub> nanoflowers as an electron donor may play a dominating role in the ultrafast and superhigh adsorption (Fig. S7) (Hazafy et al. 2011; Xiao and Pignatello 2015). To prove this hypothesis, the effects of pH value on the adsorption performance of the MoSe<sub>2</sub> nanoflowers to the malachite green were explored as shown in Fig. S8. Clearly, an acidic environment (pH = 4) adversely affects the adsorption of the malachite green on the MoSe<sub>2</sub> nanoflowers. The introduced H<sup>+</sup> may be attracted onto the negative charged surfaces of the MoSe<sub>2</sub> nanoflowers induced via the piezoresponse to the ultrasonic vibration. As a result, the

electrostatic interaction and/or  $\pi$ – $\pi$  interaction between the aromatic malachite green and the polarized MoSe<sub>2</sub> nanoflowers were somewhat decreased, leading to a weakened adsorption.

The adsorbed malachite green on the MoSe<sub>2</sub> nanoflowers was readily released in ethanol as shown in Fig. 3a. As can be seen, about 90% of malachite green can be removed from the spent MoSe<sub>2</sub> nanoflowers by using 500 mL of ethanol. This finding suggests that the loss of the malachite green in the aqueous solution is mainly due to the adsorption instead of the decomposition by the MoSe<sub>2</sub> nanoflowers. The representative photographs of the malachite green aqueous solution with the MoSe<sub>2</sub> nanoflowers at the stages of adsorption and desorption are given in Fig. 3b.

The adsorption and desorption behaviors of the MoSe<sub>2</sub> nanoflowers were studied by using SEM, XRD and FTIR, respectively. SEM image of the spent MoSe<sub>2</sub> nanoflowers after removing the absorbed malachite green is given in Fig. 3c, showing no obvious difference from the pristine one. XRD patterns of the MoSe<sub>2</sub> nanoflowers before and after removal of the absorbed malachite green shown in Fig. 3d demonstrate similar profiles, inconsistent with that of the pristine MoSe<sub>2</sub> nanoflowers in terms of the changed (002) plane. This finding indicates that the adsorption and desorption of the malachite green affect the stacking of (002) plane of the MoSe<sub>2</sub> nanoflowers. Figure 3e shows FTIR spectra of the MoSe<sub>2</sub> nanoflowers before and after removal of the absorbed malachite green. As can be seen, the characteristic bands of the malachite green appear after adsorption, and they become almost vanished after desorption. Reusability of the adsorbents is important for their practical applications. After four repeated adsorption–desorption cycles, the removal efficiency of the MoSe<sub>2</sub> nanoflowers for the malachite green is decreased up to 17% (Fig. 3f).

## Conclusion

The few-layered MoSe<sub>2</sub> nanoflowers obtained by a hydrothermal method were first discovered to have a piezoelectric effect that improves adsorption. The

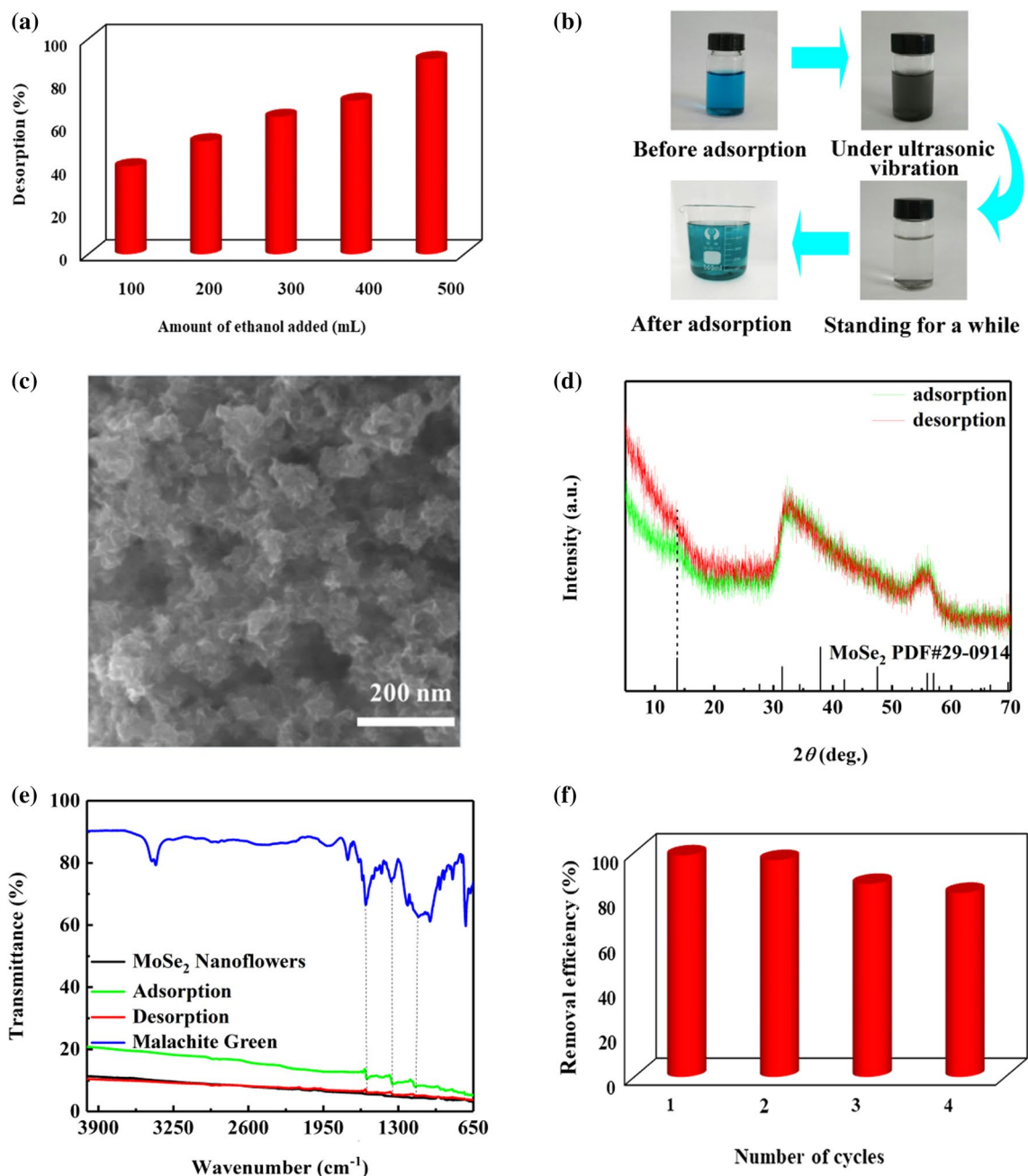


**Fig. 3** **a** Desorption of the saturated adsorbed malachite green on the MoSe<sub>2</sub> nanoflowers by using ethanol. Note that the malachite green can be completely removed by using 500 mL of ethanol. **b** Photographs of the malachite green solution with the MoSe<sub>2</sub> nanoflowers at the stages of adsorption and desorption. **c** Scanning electron microscopy (SEM) image of the MoSe<sub>2</sub> nanoflowers after saturated adsorption of the malachite green, similar to the one of the pristine MoSe<sub>2</sub> nanoflowers. **d** X-ray diffraction (XRD) patterns of the MoSe<sub>2</sub> nanoflowers after saturated adsorption of the malachite green and after desorption. Note that there is no obvious difference. **e** Fourier trans-

form infrared spectrometry (FTIR) spectra of the MoSe<sub>2</sub> nanoflowers after the saturated adsorption of the malachite green and after desorption. Note that the typical bands of malachite green appear for the MoSe<sub>2</sub> nanoflowers after adsorption and disappear after desorption, indicating the occurrence of adsorption and desorption. **f** Recycling of the MoSe<sub>2</sub> nanoflowers for the removal of the malachite green. Note that after four adsorption–desorption cycles, the removal efficiency of the MoSe<sub>2</sub> nanoflowers for the malachite green is slightly decreased

adsorption is a spontaneous physisorption process, following pseudo-second-order kinetics with the rate constant of 0.69 g mg<sup>-1</sup> min<sup>-1</sup> and Langmuir model with the theoretical

maximum adsorption capacity of 208.3 mg g<sup>-1</sup>. The ultrafast and superhigh adsorption performance of the MoSe<sub>2</sub> nanoflowers is ascribed to the presence of the electric field when

the mechanical force is exerted. Consequently, the aromatic malachite green molecules are readily adsorbed on the polarized surfaces of the MoSe<sub>2</sub> nanoflowers. This is the first report about the excellent adsorption ability of the MoSe<sub>2</sub> nanoflowers related to the piezoelectric property. This work opens up a new research window on the adsorption activity through the unique piezoeffect of the non-centrosymmetric 2D MoSe<sub>2</sub>.

**Funding** This work was supported by the National Natural Science Foundation of China (No. 51671074) and the Natural Science Foundation of Heilongjiang Province (No. LH2019F026).

## References

- Anirudhan TS, Radhakrishnan PG (2011) Thermodynamics of chromium(III) adsorption onto a cation exchanger derived from saw dust of Jack wood. *Environ Chem Lett* 9:121–125. <https://doi.org/10.1007/s10311-009-0255-5>
- Consolin-Filho N, Carvalho ER, Kamogawa MY, Martin-Neto L (2010) Copper(II) adsorption studies using models of synthetic humic acids. *Environ Chem Lett* 8:179–184. <https://doi.org/10.1007/s10311-009-0206-1>
- Duerloo KN, Ong MT, Reed EJ (2012) Intrinsic piezoelectricity in two-dimensional materials. *J Phys Chem Lett* 3:2871–2876. <https://doi.org/10.1021/jz3012436>
- Duerloo KN, Reed EJ (2015) Structural phase transitions by design in monolayer alloys. *ACS Nano* 10:289–297. <https://doi.org/10.1021/acsnano.5b04359>
- Eddingsaas NC, Suslick KS (2006) Light from sonication of crystal slurries. *Nature* 44:163. <https://doi.org/10.1038/444163a>
- Hazafy D, Salvia M, Mills A, Hutchings MG, Evstigneev MP, Parkinson JA (2011) NMR analysis of Nile blue (C. 1. basic blue 12) and Thionine (C. 1. 52000) in solution. *Dyes Pigments* 88:315–325. <https://doi.org/10.1016/j.dyepig.2010.07.014>
- Jensen K, Weldon J, Garcia H, Zettl A (2007) Nanotube radio. *Nano Lett* 7:3508–3511. <https://doi.org/10.1021/nl073089g>
- Jiang Q, Lu Y, Huang Z, Hu J (2017) Facile solvent-thermal synthesis of ultrathin MoSe<sub>2</sub> nanosheets for hydrogen evolution and organic dyes adsorption. *Appl Surf Sci* 402:277–285. <https://doi.org/10.1016/j.apsusc.2017.01.049>
- Kong Q, Preis S, Li L, Luo P, Wei C, Li Z, Hu Y, Wei C (2020) Relations between metal ion characteristics and adsorption performance of graphene oxide: a comprehensive experimental and theoretical study. *Sep Purif Technol* 232:115956. <https://doi.org/10.1016/j.seppur.2019.115956>
- Lee SW, Lee DS, Morjan RE, Jhang SH, Sveningsson M, Nerushev OA, Park YW, Campbell EEB (2004) A three-terminal carbon nanorelay. *Nano Lett* 4:2027–2030. <https://doi.org/10.1021/nl049053v>
- Li W, Li J (2015) Piezoelectricity in two-dimensional group-III monochalcogenides. *Nano Res* 8:3796–3802. <https://doi.org/10.1007/s12274-015-0878-8>
- Milošević I, Nikolić B, Dobardžić E, Damnjanović M, Popov I, Seifert G (2007) Electronic properties and optical spectra of MoS<sub>2</sub> and WS<sub>2</sub> nanotubes. *Phys Rev B* 76:1–9. <https://doi.org/10.1103/PhysRevB.76.233414>
- Nath M, Rao CNR (2001) MoSe<sub>2</sub> and WSe<sub>2</sub> nanotubes and related structures. *Chem Commun* 21:2236–2237. <https://doi.org/10.1039/B107296J>
- Ong MT, Reed EJ (2012) Piezoelectricity in graphene. *ACS Nano* 6:1387–1394. <https://doi.org/10.1021/nn204198g>
- Prathap K, Namasivayam C (2010) Adsorption of vanadate(V) on Fe(III)/Cr(III) hydroxide waste: pH effect and thermodynamics study. *Environ Chem Lett* 8:363–371. <https://doi.org/10.1007/s10311-009-0234-x>
- Stampfer C, Jungen A, Linderman R, Obergfell D, Roth S, Hierold C (2006) Nano-electromechanical displacement sensing based on single-walled carbon nanotubes. *Nano Lett* 6:1449–1453. <https://doi.org/10.1021/nl0606527>
- Timóteo VW, Spaoloni PM, Farias MB (2020) Removal of endocrine disruptors in waters by adsorption, membrane filtration and biodegradation: a review. *Environ Chem Lett*. <https://doi.org/10.1007/s10311-020-01000-1>
- Uslu H, Datta D, Bamufleh HS (2017) Zn<sup>2+</sup> Ion adsorption from aqueous solution using montmorillonite clay impregnated with Trin. *J Chem Eng Data* 62:2155–2162. <https://doi.org/10.1021/acs.jced.7b00254>
- Wu J, Li B, Shao Y, Wu X, Sun Y (2020) Tuning the morphology and phase of MoSe<sub>2</sub> by using a mixed solvent of water and dimethyl formamide and its enhanced electrocatalytic activity for hydrogen evolution reaction. *J Mater Sci* 55:2129–2138. <https://doi.org/10.1007/s10853-019-04084-5>
- Wu W, Wang L, Li Y, Zhang F, Lin L, Niu S, Chenet D, Zhang X, Hao Y, Heinz TF, Hone J, Wang Z (2014) Piezoelectricity of single-atomic-layer MoS<sub>2</sub> for energy conversion and piezotronics. *Nature* 514:470–474. <https://doi.org/10.1038/nature13792>
- Wu M, Lee J, Chung YJ, Srinivaas M, Wu J (2017) Ultrahigh efficient degradation activity of single- and few-layered MoSe<sub>2</sub> nanoflowers in dark by piezo-catalyst effect. *Nano Energy* 40:369–375. <https://doi.org/10.1016/j.nanoen.2017.08.042>
- Wu Y, Zhan S, Xu L, Shi W, Xi T, Zhan X, Zhou P (2011a) A simple and label-free sensor for mercury(II) detection in aqueous solution by malachite green based on a resonance scattering spectral assay. *Chem Commun* 47:6027. <https://doi.org/10.1039/C1CC10563A>
- Wu T, Cai X, Tan S, Li H, Liu J, Yang W (2011b) Adsorption characteristics of acrylonitrile, p-toluenesulfonic acid, 1-naphthalenesulfonic acid and methyl blue on graphene in aqueous solutions. *Chem Eng J* 173:144–149. <https://doi.org/10.1016/j.cej.2011.07.050>
- Xiao F, Pignatello JJ (2015) pi(+)-pi Interactions between (hetero) aromatic Amine Cations and the graphitic surfaces of pyrogenic carbonaceous materials. *Environ Sci Technol* 49:906–914. <https://doi.org/10.1021/es5043029>
- Xu J, Wang L, Zhu Y (2012) Decontamination of bisphenol a from aqueous solution by graphene adsorption. *Langmuir* 28:8418–8425. <https://doi.org/10.1021/la301476p>
- Yin Y, Zhang Y, Gao T, Yao T, Zhang X, Han J, Wang X, Zhang Z, Xu P, Zhang P, Cao X, Song B, Jin S (2017) Synergistic phase and disorder engineering in 1T-MoSe<sub>2</sub> nanosheets for enhanced hydrogen. *Adv Mater* 29:1700311. <https://doi.org/10.1002/adma.20170311>
- Zhang J (2019) On the piezopotential properties of two-dimensional materials. *Nano Energy* 58:568–578. <https://doi.org/10.1016/j.nanoen.2019.01.086>
- Zheng D, Zhao Z, Huang R, Nie J, Li L, Zhang Y (2017) High-performance piezo-phototronic solar cell based on two-dimensional materials. *Nano Energy* 32:448–453. <https://doi.org/10.1016/j.nanoen.2017.01.005>

**Publisher's Note** Springer Nature remains neutral with regard to jurisdictional claims in published maps and institutional affiliations.